Nonlinear supratransmission

F. Geniet, J. Leon
Physique Mathématique et Théorique, CNRS-UMR 5825
34095 MONTPELLIER (FRANCE)

March 4, 2003

Abstract

A nonlinear system possessing a natural forbidden band gap can transmit energy of a signal with a frequency in the gap, as recently shown for the nonlinear chain of coupled pendula [Phys Rev Lett 89 (2002) 134102]. This process of *nonlinear supratransmission*, occurring at a threshold exactly predictable in many cases, is shown to have a simple experimental realization with a mechanical chain of pendula coupled by a coil spring. It is then analyzed in more detail by first going to different (non-integrable) systems which do sustain nonlinear supratransmission. Then a Josephson transmission line (one dimensional array of short Josephson junctions coupled through super-conducting wires), is shown to sustain also nonlinear supratransmission, though being related to a different class of boundary conditions, and despite the presence of damping, finiteness and discreteness. Finally the mechanism at the origin of nonlinear supratransmission is a nonlinear instability, and it is briefly discussed here.

1 Introduction

It has been recently demonstrated that, in addition to energy spectral localization (the Fermi-Pasta-Ulam recurrence phenomenon [1]) and to energy spatial localization (soliton generation from initial data [2, 3, 4, 5]), a nonlinear chain of oscillators possess another striking fundamental property called *nonlinear supratransmission* [6]. This phenomenon was shown to occur in the nonlinear sine-Gordon chain, which possess a natural forbidden band gap, when it is submitted to irradiation at a frequency in the stop gap. While in a linear chain the signal would exponentially vanish in the medium, it does not do so in the nonlinear case if its amplitude exceeds a threshold value.

In [6] the irradiation of the medium was modelized by prescribing the boundary value at one end of the chain. It is worth mentioning that nonlinear transmission does occur also in the case of a true wave scattering, namely when a monochromatic plane wave scatters onto a nonlinear medium with a frequency in the gap [7].

In the case of the sine-Gordon model, the threshold can be predicted exactly by invoking the static one-breather solution [6]. In short, energy penetrates the medium as soon as the amplitude A of the harmonic driving, at a frequency Ω in the gap, exceeds the maximum amplitude of the static breather of frequency Ω. This energy travels then through the medium by means of nonlinear localized excitations (kinks, breathers, solitons).

The purpose of this paper is, after recalling results of [6], to display experimental results on the mechanical chain of pendula and to discuss the generality of our result by exploring extensions to different situations. We shall in particular explore the robustness of nonlinear supratransmission when the medium experiences damping, different nonlinearities and different classes of boundary values.

The next section is devoted to a short reminder of the results published in [6] and it is intended to settle formalism and basic facts about nonlinear supratransmission. The model is the sine-Gordon chain submitted to a Dirichlet condition at the origin on a vanishing initial background (pendula at rest). Then section 3 relates the experiment made with a mechanical pendula chain, coupled by means of a coil spring, and which is forced at one end by a periodic torque. A systematic exploration of the chain response in a frequency range within the gap shows spectacular agreement with the theory. In section 4 we numerically describe the characteristics of the breathers generated in the sine-Gordon chain and discover some simple relations between the parameters of the emitted breather with respect to those of the boundary driving. The section 5 deals with the energy transmitted by the nonlinear medium as a function of the driving amplitude at given frequency in the gap. Particular emphasis will be put on the effectiveness of the effect in different, not necessarily integrable, cases. The nonlinear instability which is the generating mechanism of nonlinear supratransmission is briefly discussed in section 6. Although the mathematical analysis is still to be constructed we propose a quite simple illustration of the process by a perturbative analysis of the sine-Gordon system driven close to a breather mode.

As another domain of study, we consider in section 7 the sine-Gordon model for Neumann conditions at the boundary (the derivative at the origin is prescribed). This is a model for a chain of short Josephson junctions whose first one is submitted to an external AC current. By using numerical simulations, the process of nonlinear supratransmission is shown to hold, and the threshold of energy transmission to obey a similar simple rule. Remarkably, in this case the energy flows by means of kink (or anti-kinks) and not by breathers (or kink anti-kink pairs). This is an interesting issue in view of applications as kinks are the objects that have an experimental signature (through the Josephson current).

2 The sine-Gordon chain

2.1 Generalities

The following normalized discrete sine-Gordon chain of N locally damped coupled oscillators $u_n(t)$

$$\ddot{u}_n - c^2(u_{n+1} - 2u_n + u_{n-1}) + \sin u_n = -\gamma(n)\dot{u}_n, \quad n = 1, \cdots, N \ , \tag{1}$$

is submitted to the boundary value at the origin (Dirichlet condition)

$$u_0(t) = A \sin \Omega t, \tag{2}$$

acting on a medium initially at rest, namely

$$u_n(0) = 0, \quad \dot{u}_n(0) = 0. \tag{3}$$

In this section the damping coefficient γ is used to model a semi-infinite chain by an absorbing boundary. More precisely we take $u_{N+1}(t) = 0$ with

$$\begin{aligned} &0 \geq n \leq m \ : \ \gamma(n) = 0, \\ &m < n \leq N \ : \ \gamma(n) = a[1 + \tanh(\frac{2n - m - N}{2b})], \end{aligned} \tag{4}$$

where the parameter b is adjusted to have a damping factor $\gamma(n)$ varying slowly from almost 0 to almost $2a$ on the last $(N - m)$ particles. A typical experiment will have e.g. $N = 100$, $m = 60$, $a = 0.5$ and $b = 3$. Note that in section 7 we shall use instead the reflective boundary condition $u_{N+1} = u_N$ for an homogeneous damping $\gamma(n) = cste$ for all n.

The equation (1) is considered as a second-order ordinary differential system for the N coupled oscillators $u_n(t)$. This system is then solved with the subroutine `dsolve` of `MAPLE` software package which uses a Fehlberg fourth-fifth order Runge-Kutta method.

2.2 Forcing in the gap

The linear dispersion relation $\omega(k)$ of the chain is

$$\omega^2 = 1 + 2c^2(1 - \cos k). \tag{5}$$

For a driving boundary (2) with frequency in the forbidden band gap (FBG), namely $\Omega < 1$, a linear chain would sustain the solution (evanescent wave)

$$A \sin(\Omega t) \exp[-\lambda n]. \tag{6}$$

The parameter λ is given from the dispersion relation (5) written for $\omega = \Omega < 1$ and $k = i\lambda$, namely

$$\lambda = \text{arccosh}\left(1 + \frac{1 - \Omega^2}{2c^2}\right). \tag{7}$$

In the nonlinear case, in order to fit the boundary condition (2), the *approximate* solution (exact in the continuous limit) is given instead by the static breather

$$u_b(n,t) = 4 \arctan \left[\frac{\lambda c \sin(\Omega t)}{\Omega \cosh(\lambda(n-n_0))} \right], \tag{8}$$

where the breather center n_0 solves

$$A = 4 \arctan \left[\frac{\lambda c}{\Omega \cosh(\lambda n_0)} \right]. \tag{9}$$

The above equation expresses that the static breather fits the driving field (2) by adjusting its position such as to match the amplitude A. The spectrum of the breather signal does not match exactly the monochromatic forcing (2) and it adapts by sending phonons at third, fifth, etc..., harmonic frequencies.

The above assertion is checked by performing two simulations of (1) at a given forcing frequency, say $\Omega = 0.8$, and a given amplitude, say $A = 2$, in one case with the harmonic forcing (2), in the other case with the breather-like forcing $u_b(0,t)$ where the value of n_0 is calculated from (9) with $A = 2$. To avoid initial shock we also set initial velocities matching the ones of the static breather. Then we evaluate by Fourier transform the spectra of one particle of the chain in both cases (we have selected the particle 50 on a chain of 100 pendula). The result is displayed on figure 1 where we see that phonons at frequency 3Ω are indeed emitted for harmonic forcing while no phonon appear for a breather-like forcing. The small contribution at frequency 1 in figure (a)

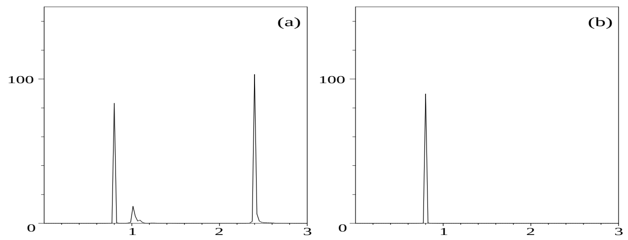

Figure 1: Spectra of the particle 50 submitted to, (a) harmonic boundary driving at frequency 0.8 and amplitude 2 and to, (b) breather boundary driving at frequency 0.8.

represents a collective motion of the pendula generated by the initial shock resulting from inadequation of the initial velocities with the boundary value.

2.3 Bifurcation threshold

The adjustment of the breather center n_0 provided by (9) not always has a solution. Indeed it works up to the maximum value $A = A_s$ of the breather amplitude realized for $n_0 = 0$. Beyond this threshold, for a driving boundary with $A > A_s$, we have shown in [6] that nonlinear supratransmission occurs, i.e. the medium starts to transmit energy by means of nonlinear modes generation (breathers and kink-antikink pairs). From (8), the threshold A_s reads as the following function of the frequency Ω

$$A_s = 4 \arctan \left[\frac{c}{\Omega} \text{arccosh} \left(1 + \frac{1-\Omega^2}{2c^2} \right) \right], \tag{10}$$

which has the approximate value

$$A_s \sim 4 \arctan[\frac{\sqrt{1-\Omega^2}}{\Omega}]. \tag{11}$$

which would hold for the continuous sine-Gordon equation obtained in the limit $1/c \to 0$. Note that the maximum difference (when Ω varies in $[0,1]$) between the above two expressions is already 1% for $c = 1$ and goes down to 0.01% for $c = 10$, the value we have used in most of the numerical simulations.

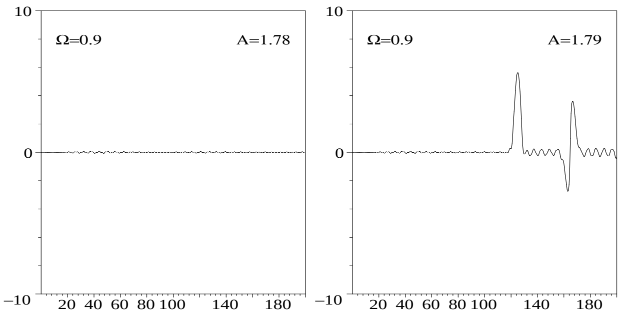

Figure 2: Representation of $u_n(t)$ as a function of time for $n = 60$ in the case $\Omega = 0.90$ for two amplitudes.

This qualitative definition of a bifurcation threshold can be checked on numerical simulations of (1) with the boundary condition (2) by varying, at given frequency Ω, the amplitude A around the above value $A_s = 1.803$ (for $c = 4$). There are many means to determine appearance of nonlinear supratransmission, a simple one being the observation of the motion of one particle of the chain. As an example we display in figure 2 the motion of the particle 60 of a chain of 200 particles driven at frequency 0.9 at amplitudes $A = 1.78$ (no supratransmission) and $A = 1.79$ (supratransmission) for a coupling factor $c^2 = 16$. Each large oscillation in the second figure corresponds to a breather passing by. Two of them are generated and cross the site 60 at times 120 and 160. The small oscillation seen between the humps are the harmonic phonons, mainly of frequency 3Ω.

For illustration we show on figure 3 a picture of oscillators amplitude $u_n(t)$ at given time (here $t = 120$) in the case of nonlinear supratransmission obtained for $A = 1.8$ and $\Omega = 0.9$. A first breather propagates to the right while a second one is just being generated near the origin. Note the amplitude of the breather with respect to the one of the driving boundary.

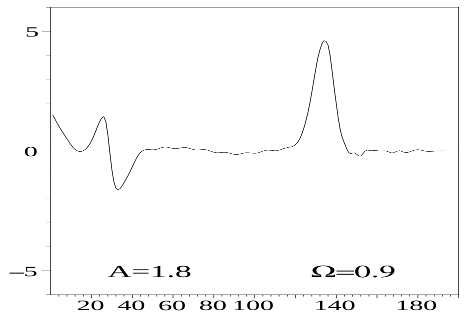

Figure 3: Plot of $u_n(t)$ as a function of n at $t = 120$.

By a systematic exploration of the chain response we draw figure 4 obtained for 200 particles with a coupling $c^2 = 100$ (some experiments have been actually made with smaller coupling and less number of points to shorten computation times) for a typical time of 200 (for frequencies close to the gap value 1, time had to be increased up to 500). The points on figure 4 are obtained with an absolute precision of 10^{-2} for the amplitude A. They are compared to the theoretical threshold expression (10) (continuous curve).

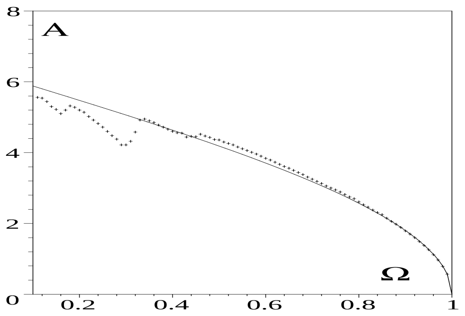

Figure 4: Bifurcation diagram in the (A, Ω) plane. The solid line is the threshold expression (10). The crosses indicate the lowest value of A for which nonlinear supratransmission is seen on numerical simulations.

The figure 4 shows excellent agreement to formula (10) apart for some discrepancies starting below 0.33 and 0.18. This results from the driving which, thanks to the nonlinearity, generates phonons at multiple frequencies (here third, fifth, etc...). If these frequencies lie in the phonon band, the phonons move away from the boundary and have no effect on the forcing. If however they lie in the FBG, the related phonons do not propagate (which we call phonon quenching) and stick on the boundary where they add contribution to the driving. This effect indeed disappears when driving the system (1) with the exact breather boundary value $u_b(0, t)$ for which we have checked that nonlinear supratransmission *never occurs* at an amplitude $A < A_s$, while it occurs already at $A = A_s$

(or for very small deformation of the perfect breather).

3 Experiments on a mechanical chain

Our purpose here is to show that the process of nonlinear supratransmission can be easily realized experimentally on a chain of coupled pendula as depicted in figure 5. This chain has been built following M. Remoissenet [5]. The pendula rotate freely around a piano wire stretched between two supports, they are coupled together by a coil spring tightened to each pendulum by a screw.

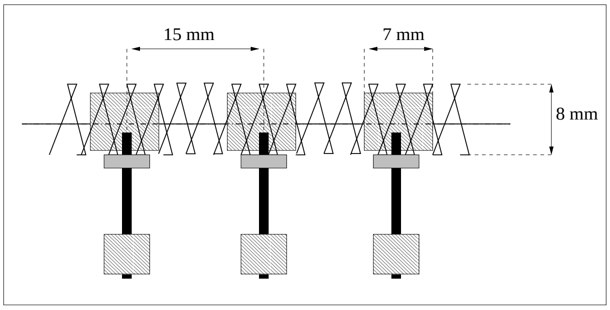

Figure 5: Sketch of the mechanical chain.

Such a chain of 48 pendula is driven by an electrical engine steered by a generator of sinusoidal tension. Upon varying the frequency, at low amplitude, in the phonon band, we can determine the parameters of the chain (coupling constant σ^2 and angular eigenfrequency ν_0) by measuring the wavelength $2\pi/k$ of produced wave (in units of pendula number). By comparison to the dispersion relation of the linear chain

$$\nu^2 = \nu_0^2 + 2\sigma^2(1 - \cos k). \tag{12}$$

we determined the following parameter values

$$\nu_0 = 15 \text{ Hz} \ , \quad \sigma = 32 \text{ Hz} \tag{13}$$

Then in a time normalized to the eigenfrequency, we have the dispersion relation (5) with

$$c = \frac{\sigma}{\nu_0} = 2.13, \tag{14}$$

which is the fundamental parameter of the model, entering in particular expression (10) of the threshold amplitude for nonlinear supratransmission. This is the formula we want here to confront to experiments.

We proceed with a systematic exploration of the chain response to a signal frequency in the gap (of value less than ν_0). The method consist in increasing slowly, at fixed frequency, the amplitude of the driving, up to the time when a

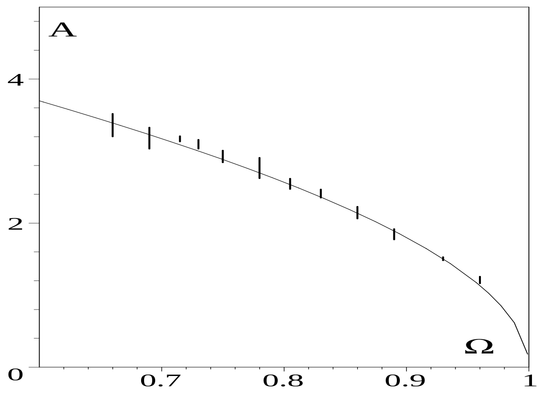

Figure 6: Experimental values of nonlinear supratransmission threshold compared to expression (10).

nonlinear mode is seen to be generated (a picture of a breather generated at a frequency of 0.85 in normalized units is displayed in [6]). Repeating 3 times, for each driving frequency value, the measurements of the driving amplitude that generates a nonlinear mode, we eventually obtain the figure 6 which displays the measured threshold amplitude in terms of the signal frequency (normalized). There, the full line curve is the function $A_s(\Omega)$ given in (10) with $c = 2.13$.

Despite the small number of pendula, inducing reflection at the open end, the inherent damping, and other mechanical imperfections, the experiments provide a spectacular realization of the theoretical threshold prediction.

4 Characteristics of the emitted breathers

One important issue concerns the nature and the characteristics of the nonlinear modes which propagate in the medium. In the first instance, we have to check that the emitted structures correctly match the moving breather, at velocity $v < 1$, which is convenient to write as

$$u_v(n,t) = 4 \arctan \left[\frac{r \sin\left(\frac{1}{\sqrt{1+r^2}} \frac{t - vn/c}{\sqrt{1-v^2}}\right)}{\cosh\left(\frac{r}{\sqrt{1+r^2}} \frac{n/c - vt)}{\sqrt{1-v^2}}\right)} \right] . \qquad (15)$$

By choosing correctly the two parameters r and v which represent respectively the amplitude and the group velocity of the breather, together with the space and time origins of the solution $u_v(n - n_0, t - t_0)$, one can match it to the asymptotic numerical solution with high precision. This enables us to identify correctly the emitted breathers, to determine their characteristic with a great accuracy, and to observe their possible disintegration into kink-antikink pairs.

The results of such estimations are displayed in figure 7 obtained as follows. For each driving frequency Ω, we have driven the system at threshold amplitude $A_s(\Omega)$ and then determined at the the parameters $\{r, v\}$ of the emitted breathers (a given experiment at threshold driving produces repeatedly the same breather). Then the amplitude of the propagating breather is plotted as a function of the amplitude of excitation $A_s(\Omega)$ for various frequencies. Similarly, figure 8 shows the group velocity of the breather as a function of $A_s(\Omega)$.

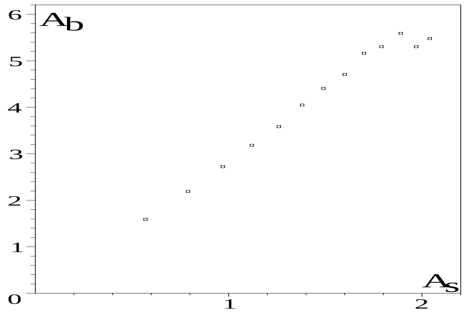

Figure 7: Amplitude of the emitted breathers in terms of the amplitude of excitation, just above the emission threshold.

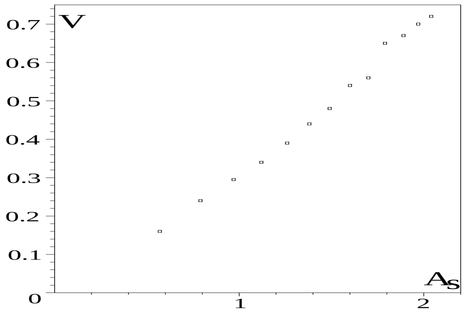

Figure 8: Group velocity of the emitted breathers, as a function of the amplitude of excitation, just above the emission threshold.

Both figures 7 and 8 correspond to a region of the driving frequency close to the gap $0.87 \leq \Omega \leq 1$. For lower frequencies the emitted breathers, when they occur, are unstable and decay into kink-antikink pairs (this will be discussed later). The main conclusion here is the existence of a linear relation between the amplitude A_b (and the velocity v) of the generated breather and the driving amplitude at threshold A_s. So far we have no theoretical interpretation of these observations.

Another characteristic of the breather is its proper frequency ω_b, related to the apparent pulsation period T by the usual (relativistic) relation

$$\omega_b = \frac{1}{\sqrt{1+r^2}} = \frac{2\pi}{T\sqrt{1-v^2}} \ . \tag{16}$$

This frequency is plotted in figure 9 as a function of the driving frequency Ω and, again, we note a non trivial linear dependence.

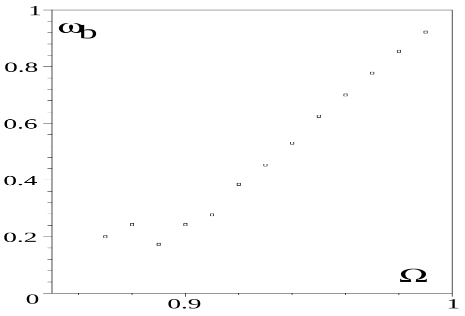

Figure 9: Proper frequency of the emitted breathers, as a function of the driving frequency Ω, just above the emission threshold.

We now turn to the stability of the emitted breathers which, for $\Omega \leq 0.88$ decay into kink-antikink pairs. This can be qualitatively described by studying the binding energy W, given by

$$W = 2E_k - E_b = \frac{16}{\sqrt{1-v^2}} \left(1 - \sqrt{\frac{r^2}{1+r^2}} \right) , \tag{17}$$

where E_k is the single kink energy and E_b the breather energy [5].

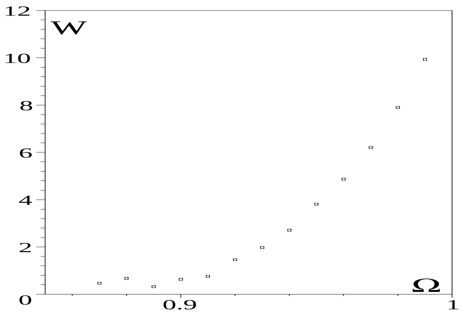

Figure 10: Binding energy of the emitted breathers, as a function of the frequency of excitation, just above the emission threshold.

We have evaluated the binding energy W of the breathers produced in the simulations (by plugging in (17) the measured values of r and v), the result of which is plotted in figure 10 in terms of the frequency Ω of the driving boundary. This figure shows that the binding energy of the breather decreases with the driving frequency, and goes to zero for $\Omega \lesssim 0.88$. Thus the breather decay in the frequency range $[0, 0.8]$ is well understood from formula (17).

5 Energy transmission

5.1 Basic expression

Nonlinear supratransmission is a process where large amount of energy flows through the medium. Our purpose here is to evaluate numerically this energy for amplitudes around the threshold value. The theoretical expression of the energy flow is calculated hereafter for a generic nonlinearity deriving from a potential energy $V(u_n)$ (the sine-Gordon case (1) corresponds to $V(u_n) = 1 - \cos u_n$).

From the energy density

$$H_n = \frac{1}{2}\dot{u}_n^2 + \frac{c^2}{2}(u_{n+1} - u_n)^2 + V(u_n), \quad n = 1, \cdots \infty \ , \tag{18}$$

and the evolution equation follow the conservation law

$$\frac{\partial}{\partial t}H_n + (J_{n+1} - J_n) = 0, \tag{19}$$

with the current

$$J_n = -c^2 \dot{u}_n (u_n - u_{n-1}). \tag{20}$$

Incorporating the potential energy resulting from the coupling of the first particle u_1 to the boundary u_0, the *total energy* of the system reads

$$E = \sum_{n=1}^{\infty} H_n + \frac{c^2}{2}(u_1 - u_0)^2. \tag{21}$$

In our case $u_0(t)$ is the driving (2) and the chain is supposed infinite with $u_n(t) \to 0$ as $n \to \infty$.

Upon time derivation, with help of the conservation law, and using the assumed asymptotic $J_n \to 0$ for large n, we arrive eventually at

$$\frac{\partial}{\partial t}E = c^2 \dot{u}_0 (u_0 - u_1). \tag{22}$$

Hence the total energy injected in the medium during time T reads

$$E = c^2 \int_0^T dt \ \dot{u}_0(t)[u_0(t) - u_1(t)]. \tag{23}$$

Choosing for T an integer multiple of the period of excitation makes this energy to vanish identically in the linear case if the driving frequency falls in the FBG.

5.2 Numerical simulations

In the nonlinear case, expression (23) is computed numerically on a chain of 60 particles with a coupling parameter $c^2 = 16$ and an absorbing end working over the last 40 particles. For a driving frequency 0.9 and amplitudes running from

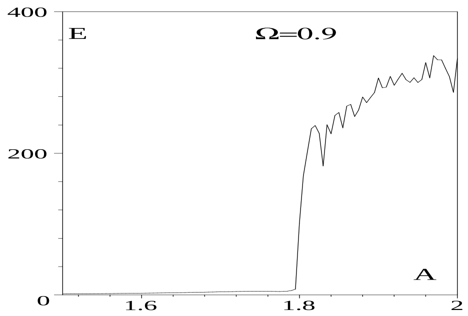

Figure 11: Energy E injected in the sine-Gordon nonlinear chain for $T = 140$ as a function of the driving amplitude A.

1.5 to 2.0, we obtain the figure 11 where the bifurcation is seen to occur for $A = 1.80$, the value predicted by formula (10). This simulation has been run for frequencies in the range $[0.2, 0.9]$, with comparable expected results.

Our approach stems from the existence of a breather solution of the model equation, allowing to determine the threshold amplitude. It is then worth wondering if the process is robust *against* non-integrability.

To give a partial still instructive answer to this question, we have performed numerical simulations of two non-integrable evolution in the same class, i.e. with Hamiltonian (18).

First the Taylor truncated expansion of sine-Gordon (fifth order is kept to ensure a confining potential at large u_n) reads as the nonlinear Klein-Gordon chain:

$$\ddot{u}_n - c^2(u_{n+1} - 2u_n + u_{n-1}) + u_n - \frac{1}{3!}u_n^3 + \frac{1}{5!}u_n^5 = 0, \quad n = 1, \cdots, N \ . \quad (24)$$

This system is solved with the boundary driving (2) and the energy (23) is computed for the same parameter values as for figure 11. The result is displayed on figure 12.

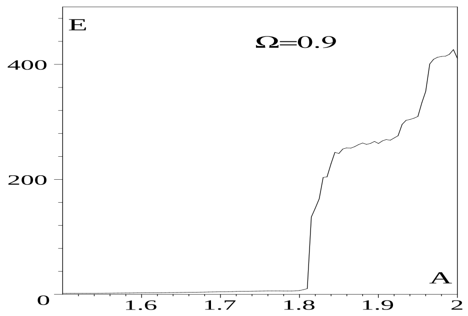

Figure 12: Energy in the Klein-Gordon chain (24).

By scanning the frequency range in the gap, we have obtained that the process occurs down to $\Omega = 0.7$ and then disappears. We suspect that for such a polynomial potential energy, at high forcing amplitude, the *incoming wave* sees an almost parabolic potential, while for low amplitude driving the *incoming wave* does feel the actual structure of the local potential.

Another interesting non integrable Hamiltonian evolution where the local potential has a periodic structure is the double sine-Gordon chain

$$\ddot{u}_n - c^2(u_{n+1} - 2u_n + u_{n-1}) + \frac{1}{3}[\sin u_n + \sin 2u_n] = 0, \quad n = 1, \cdots, N \ . \quad (25)$$

Once again we have solved this system in the same situation as before and obtained the brutal energy flow of figure 13. In this case the process holds for any frequency (tested from $\Omega = 0.2$) just as in the sine-Gordon case.

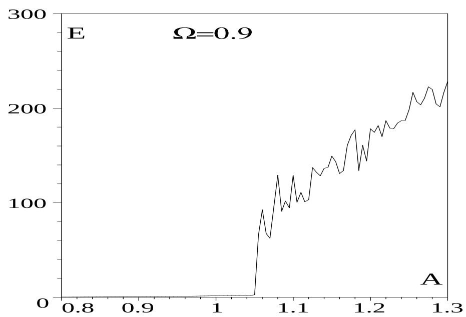

Figure 13: Energy in the double sine-Gordon chain (25).

Thus we have seen that in those two cases nonlinear supratransmission does work which is a strong indication that it is a generic nonlinear process. An interesting question is the mechanism that generates nonlinear supratransmission, which is discussed now.

6 Generating instability

The process at the origin of nonlinear supratransmission is a nonlinear instability. Although it is not yet fully understood, we discuss here some of its relevant aspects.

To that end we explore the properties of the sine-Gordon chain (1) submitted to initial-boundary value data that precisely mimic the breather $b_n(t)$ centered at $n_0 = 0$ as defined in (8) and which is convenient to write as

$$b_n(t) = 4 \arctan \phi_n(t) \ , \quad (26)$$

$$\phi_n(t) = \frac{\lambda c}{\Omega} \frac{\sin \Omega t}{\cosh \lambda n} \ . \quad (27)$$

Note that this is an exact solution in the continuous limit $1/c \ll 1$ and $\{x = n/c,\ \lambda c = \kappa,\ \Omega^2 = 1 - \kappa^2\}$.

In order to study the behavior at the threshold, we impose the boundary value

$$u_0(t) = (1+\epsilon)b_0(t) \ , \tag{28}$$

together with compatible initial data

$$\begin{aligned} u_n(0) &= (1+\epsilon)b_n(0) \ , \\ \dot{u}_n(0) &= (1+\epsilon)\dot{b}_n(0) \ . \end{aligned} \tag{29}$$

The boundary value at the other end of the chain ($n = N$) can be taken as an absorbing end to simulate the infinite line or as the breather value $b_N(t)$, e.g. to check the accuracy of the solution.

The parameter ϵ measures the departure from the exact solution. We are of course interested in what happens when ϵ is positive. For $\epsilon = 0$ we simply generate the approximate solution $b_n(t)$ which in the numerical simulations is marginaly stable (and would be indeed stable for a breather centered in $n_0 < 0$).

In the case $\epsilon > 0$, the numerical simulations of the sine-Gordon model immediately generate nonlinear supratransmission. From the initial-boundary value problem, it is natural to seek a solution as a perturbation of the breather under the form

$$u_n(t) = b_n(t) + \epsilon\eta_n(t) \ , \tag{30}$$

which by (1) obeys at order 1 in ϵ

$$\ddot{\eta}_n - c^2(\eta_{n+1} - 2\eta_n + \eta_{n-1}) + C_n\eta_n = \epsilon D_n\eta_n^2 \ . \tag{31}$$

The variable coefficients $C_n(t)$ and $D_n(t)$ of this equation are given by

$$\begin{aligned} C_n &= \cos b_n = 1 - \frac{8\phi_n^2}{(1+\phi_n^2)^2} \ , \\ D_n &= \frac{1}{2}\sin b_n = 2\phi_n\frac{1-\phi_n^2}{(1+\phi_n^2)^2} \ . \end{aligned} \tag{32}$$

The initial-boundary value problem that goes with (31) can be taken to results from (28), namely

$$\eta_0(t) = b_0(t) \ , \tag{33}$$

with the related initial data. Then we observe the following fundamental facts:

- for $\epsilon < 0$ the system (31) is stable showing a long period oscillatory behavior,
- for $\epsilon > 0$ the system is unstable showing an exponential growth of the oscillations.

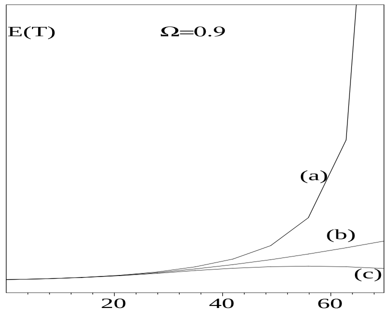

Figure 14: Energy $E(T)$ given by (23) computed for the chain (31). (a) exponential growth for $\epsilon = 0.005$, (b) linear growth for $\epsilon = 0$ and (c) oscillations for $\epsilon = -0.005$. $E(T)$ varies here on the scale $[0, 2\ 10^4]$.

These observations are illustrated by figure 14 where we have computed the energy transmitted by the chain (31) according to formula (23), as a function of time (the points in time are chosen as integer multiples of the period $2\pi/\Omega$). The parameters related to this experiments are $N = 100$, $c = 10$ and the energy has been calculated for 10 points (up to $t = 20\pi/\Omega$). We have also displayed results for the *linear version* of system (31) (read with $\epsilon = 0$) which is marginaly unstable showing a linear growth of the oscillations. The exponential growth in the case $\epsilon > 0$ is the signature of the instability which is the mechanism of nonlinear supratransmission. The mathematical approach of this instability for (31) is reported to future studies.

7 Josephson junctions array

7.1 The model

A Josephson junction behaves just like a single pendulum, the rotation amplitude being replaced by the phase difference between wave functions of Cooper pairs [8]. By connecting the Junctions in parallel with super-conducting wires, the resulting model equation is just the sine-Gordon discrete system submitted to damping and constant torque [9]

$$\ddot{u}_n + \gamma \dot{u}_n + \sin u_n = J + c^2(u_{n+1} - 2u_n + u_{n-1}), \quad n = 1, \cdots, N\ . \qquad (34)$$

Here above γ is the constant damping along the array, J is the normalized intensity of the applied current and time has been normalized to the plasma frequency.

We consider here only the one-dimensional geometry but it is worth mentioning the coupled arrays (ladders) who revealed as a means to generate discrete breathers by convenient initial conditions [10] with subsequent striking experimental realizations [11].

The applied current can have a DC component (the so-called bias) and an AC driving part. The problem we are interested in is the behavior of the above chain initially at rest and whose first junction only is submitted to AC driving at a frequency Ω in the gap and intensity I. Then the model results as (34) for $n > 1$ and the bias $J = I_0$ together with the following relation for $n = 1$:

$$\ddot{u}_1 + \gamma \dot{u}_1 + \sin u_1 = c^2(u_2 - u_1) + I_0 + I \sin \Omega t. \tag{35}$$

It is important to remark that the above equation can be equivalently written as the *discrete Neumann condition*

$$c(u_1 - u_0) = -\frac{I}{c} \sin \Omega t, \tag{36}$$

when the system (34) is assumed to hold also for $n = 1$. This remark actually allows us to consider the continuous limit in order to determine the prediction of the threshold of nonlinear supratransmission.

7.2 Bifurcation threshold prediction

The continuous version of (34) and boundary value (36), for the variable $x = n/c$ and $c \to \infty$, reads as the system

$$u_{tt} + \gamma u_t + \sin u = I_0 + u_{xx}, \tag{37}$$

$$\partial_x u|_{x=0} = B \sin \Omega t, \tag{38}$$

where we have defined $B = -I/c$. This continous version corresponds to a long Josephson junction whose extremity $x = 0$ is submitted to external micro-wave irradiation, the amplitude B being then related to the external magnetic field intensity [12]. This is a Neumann boundary condition for the sine-Gordon continuous equation (37).

The system will then adapt the breather *derivative* at the boundary centered in $-x_0$, namely

$$\partial_x u_b|_{x=0} = 4\frac{\kappa^2}{\Omega} \frac{\sin \Omega t \; \sinh \kappa x_0}{\cosh^2 \kappa x_0 + (\kappa^2/\Omega^2) \sin^2 \Omega t}, \tag{39}$$

where now the continuous version of the dispersion relation is $\Omega^2 + \kappa^2 = 1$ for evanescent waves (due to the change of space variable, we have $\kappa = c\lambda$ where λ is defined in (7)).

Upon varying the position x_0, the above expression has a maximum value for $x_0 = x_m$ given by $\sinh^2 \kappa x_m = 1 + \kappa^2/\Omega^2$ and the related maximum amplitude of the derivative eventually results as the simple expression

$$B_s = 2(1 - \Omega^2). \tag{40}$$

This is the threshold prediction for the Neumann condition (38) and we are going now to check it on numerical simulations.

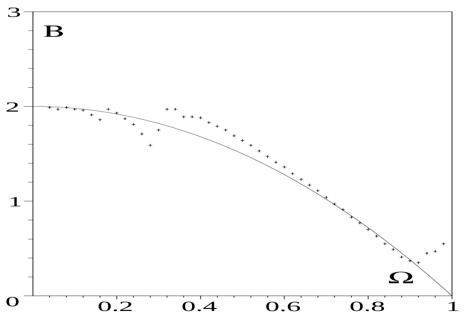

Figure 15: Bifurcation diagram in the (B, Ω) plane. The solid line is the threshold expression (40). The crosses indicate the lowest value of B for which nonlinear supratransmission occurs.

As in section 2, we solve the discrete system (34) with no constant bias ($I = 0$), without damping in a first stage ($\gamma = 0$), for a chain of 60 particles with an absorbing boundary on the last 30, and with a coupling factor $c^2 = 25$. The result is displayed on figure 15 which shows good agreement except maybe around the frequencies 0.33 and 0.18 as in figure 4 (for the same reasons) and close to the phonon band, which is due to the absorbing end.

7.3 Josephson transmission line (JTL)

Here above the situation is that of a quasi-continuous undamped and semi-infinite sine-Gordon chain submitted to Neumann condition (38) a the origin. We turn back now to the discrete case, a one-dimensional finite-length (open-ended) array of coupled short Josephson junctions, where the first pendulum is submitted to an external AC driving.

Namely we consider the *Josephson transmission line* system

$$\ddot{u}_1 + \gamma\dot{u}_1 + \sin u_1 = c^2(u_2 - u_1) + I_0 + I \sin \Omega t, \tag{41}$$

$$\ddot{u}_n + \gamma\dot{u}_n + \sin u_n = I_0 + c^2(u_{n+1} - 2u_n + u_{n-1}), \tag{42}$$

$$u_{N+1} = u_N. \tag{43}$$

Nonlinear supratransmission becomes here the property of the JTL to transmit energy under the form of kinks (or anti-kinks) as soon as the intensity I of the AC driving of the first junction exceeds the threshold

$$I_s = 2c(1 - \Omega^2) \tag{44}$$

as given by the definition $I = -cB$ and from expression (40).

A new fact here is that, for Neumann type boundary conditions as (36), only kinks (or anti-kinks) are produced, not breathers. This is the result of the fact that producing a kink cost half of the energy used to produce a breather, and of the freedom left on the boundary value $u_0(t)$ (only the difference $u_1 - u_0$ is prescribed) allowing full 2π-rotations. For Dirichlet boundary condition as in preceding sections, the precription of $u_0(t)$, e.g. by (2) prevents full rotation.

To illustrate this property we draw in figure 16 a typical simulation with the following set of parameters

$$N = 10\ , \quad \gamma = 0.1\ , \quad c = 3\ , \quad I_0 = 0.1\ , \tag{45}$$

constituting a reasonable choice for an experimental situation. At frequency $\Omega = 0.7$, the threshold (44) is $I_s = 3.06$ and for an AC driving at amplitude $I = 3.3$ the chain starts to *rotate*, which means that a number of kinks (elementary 2π rotation) are generated by the AC driving. In the case of figure 16 about 184 kinks have been generated during 1000 units of normalized time.

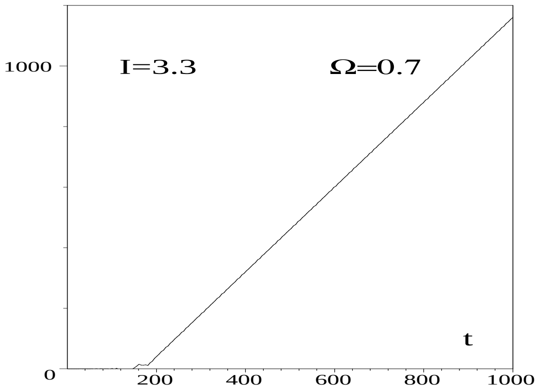

Figure 16: Motion of the particle 5 in a JTL of 10 junctions with parameters (45).

Note that we have assumed a small constant bias DC current $I_0 = 0.1$ in order to select kinks instead of possible anti-kinks. However the process does work without bias, though in some of the experiments the rotation would stop after some time (for a reason that we do not understand). Finally we mention that we have selected compatible boundary condition, namely, first an AC forcing that starts from zero and slowly reaches the value I within 100 units of time, second the following initial positions and velocities

$$u_n(0) = \arcsin(I_0)\ , \quad \dot{u}_n(0) = 0. \tag{46}$$

Then the nonlinear supratransmission does work in such JTL, despite the small number of oscillators, the presence of damping, the free-end boundary condition and the presence of constant bias.

7.4 Energy transmission

In order to compute the transmitted energy in the present situation, we start with expression (21) but written for a *finite number* N of oscillators, i.e.

$$E = \sum_{n=1}^{N} H_n + \frac{c^2}{2}(u_1 - u_0)^2. \tag{47}$$

As before, this expression is differentiated and, by use of the conservation law (19), the free boundary condition $u_{N+1} = u_N$ leads to the same result, namely

$$\frac{\partial}{\partial t}E = c^2 \dot{u}_0(u_0 - u_1). \tag{48}$$

Now, to compute the total energy injected in the medium during time T, it is necessary to use integration by parts together with the Neumann condition (36) and to chose for T an integer multiple of the period of the driving. We eventually obtain ($\ell = 20$ in the numerical simulations)

$$T = \ell \frac{2\pi}{\omega} \ , \quad E = -I\Omega \int_0^T dt \ u_1(t) \cos \Omega t \ . \tag{49}$$

This is the quantity that we have computed, for each value of the AC-driving I, in figure 17.

The bifurcation of energy translission is now quite clear on the graph of the energy $E(T)$ transmitted to the chain displayed in figure 17 obtained for $\Omega = 0.7$ and the parameters given in (45).

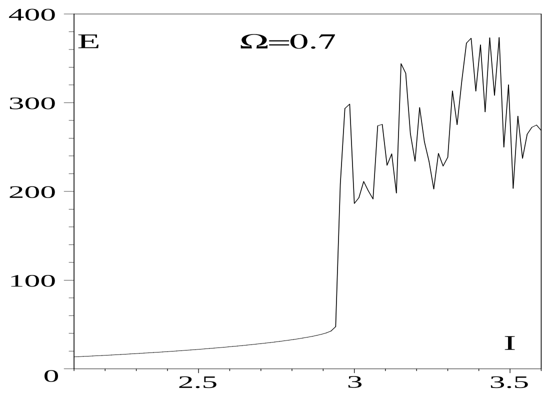

Figure 17: Energy transmitted for 180 time units by a JTL in terms of the driving intensity I.

8 Conclusion

The ability of a nonlinear medium to transmit energy when submitted to periodic boundary driving at a frequency in a stop gap and at an amplitude beyond a threshold value, which we called nonlinear supratransmission, has been shown to have some universality (so far in the domain of nonlinear wave type of equations). The process does not rely on integrability and is robust against damping, discreteness (in a reasonable range), finiteness and different classes of boundary values. The mechanism at the origin of this process is a nonlinear instability which is still under study.

Moreover, the nonlinear supratransmission has a simple experimental realization in the pendula chain which works surprisingly well. Some other experimental results are expected in Josephson transmission lines.

Acknowledgements. It is a pleasure to acknowledge enlighting discussions with M.J. Ablowitz and M. Remoissenet, A.V. Ustinov, and decisive experimental help of N. Clementin, O. Guille, P. Munier and Y. Patin.

References

[1] E. Fermi, J.R. Pasta, S.M. Ulam, *Studies of nonlinear problems*, Los Alamos Sci. Lab. Rep. (1955) LA-1940, reproduced in: A.C. Newell (Ed.) *Nonlinear wave motion*, AMS Lect Appl Math **15** (1974)

[2] C.S. Gardner, J.M. Greene, M.D. Kruskal, R.M. Miura, Phys Rev Lett **19** (1967) 1095

[3] V.E. Zakharov, A.B. Shabat, Sov Phys JETP **37** (1972) 62

[4] M.J. Ablowitz, D.J. Kaup, A.C. Newell, H. Segur, Stud Appl Math **53** (1974) 249

[5] M. Remoissenet, *Waves Called Solitons*, Springer (Berlin 1999). A.C. Scott, *Nonlinear science*, Oxford Univerity Press (New York 1999)

[6] F. Geniet, J. Leon, Phys Rev Lett 89 (2002) 134102

[7] J-G. Caputo, J. Leon, A. Spire, Phys Lett A **283** (2001) 129-135

[8] A. Barone, G.釉ternó, *Physics and Application of the Josephson Effect*, Wiley (New-York 1982). A.V. Ustinov, Physica D **123** (1998) 315

[9] H.S.J. van der Zant, M. Barahona, A.E. Duwel, T.P. Orlando, S. Watanabe, S. Strogatz, Physica D **119** (1998) 219

[10] L.M. Floria, J.L. Marin, P.J. Martinez, F. Falo, S. Aubry, Europhys Lett **36** (1996) 539. S. Flach, M. Spicci, J Phys C : cond matt **11** (1999) 321

[11] E. Trias, J.J. Mazo, T.P. Orlando, Phys Rev Lett **84** (2000) 741. P. Binder, D. Abraimov, A.V. Ustinov, S. Flach, Y. Zolotaryuk, Phys Rev Lett **84** (2000) 745

[12] A.V. Ustinov, J. Mygind, V.A. Oboznov, J Appl Phys **72** (1992) 1203. A.V. Ustinov, J. Mygind, N.F. Pedersen, V.A. Oboznov, Phys Rev B **46** (1992) 578